Portevin–Le Chatelier effect

Scott V. Franklin,* F. Mertens, and M. Marder
Center for Nonlinear Dynamics and Department of Physics, The University of Texas at Austin, Austin, Texas 78712
(Received 29 November 1999)

Aluminum subjected to smooth mechanical loading does not often deform in a correspondingly smooth manner. Typically it deforms inhomogeneously through the propagation of deformation fronts that slowly traverse the sample. These are called Portevin–Le Chatelier fronts; what determines their velocity has been somewhat mysterious. We present a phenomenological theory for deformation fronts that centers on a nonlocal rate dependence of the flow stress. In a one-dimensional idealization the equations can be solved exactly, and compared directly with experiment. Many significant features of deformation fronts are captured, including a well-known transition from hopping to continuous front motion. The phenomenology's predictions are confirmed by our experiments.

PACS number(s): 81.40.Lm, 81.05.Bx

I. INTRODUCTION

A. Motivation

Aluminum's properties, chiefly its strength and light weight, make it ideal for many commercial uses. Its usefulness is limited, however, by a series of bands that form when the metal is rolled or formed. The bands mark regions of appreciable plastic deformation; they are visible because of surface roughness on the micron scale. The bands are part of a more general phenomenon of inhomogeneous deformation in which yielding proceeds as a propagating front. The bands occur when this front ceases to move with steady velocity and begins to hop.

The bands form all too easily during metal forming, such as in die presses, but are typically studied systematically in experiments with the geometry illustrated in Fig. 1. An aluminum sample a few centimeters long, a centimeter wide, and a few millimeters thick is gripped at two ends and pulled. After stretching in a reversible and elastic fashion, the aluminum yields plastically. The nature of its deformation thereafter depends upon several factors that we will explore in this paper.

In the simplest experiments, the stress on the sample is slowly increased and bursts of yielding occur at critical stresses. This produces a ''staircase'' on a stress-strain curve, the earliest known example is shown in Fig. 2. Each vertical line corresponds to the nucleation of a deformation front.

It is more common to force one end of the sample to move at a constant velocity. The machine stiffness then becomes a factor, as the amount by which the stress can relax depends upon the relative stiffness of machine and sample. This has obscured a fundamental question: can fronts propagate under a constant stress, or do they require an ever-increasing load to move? Our experiments [1] unambiguously show the former to be true, and this behavior is reproduced in our theory.

A picture of a deformation front moving steadily through an aluminum sample is shown in Fig. 1. The fronts are typically about a millimeter wide and move at speeds of centimeters per second. Metals deform through the generation and propagation of dislocations, which appear on the submicron scale. The key to the effect lies ultimately bundled in the dynamics that connect the microscopic world of dislocations to the macroscopic regime of the fronts. However, we will not make any explicit connection to the dislocation scale in this paper. All our analysis will be purely phenomenological.

B. Historical Note

It is widely believed (e.g., [1]) that Portevin and Le Chatelier [2] were the first to study systematically the phenomenon of inhomogeneous plasticity. This is not true. Duleau commented on irregularities in the deformation of metal in 1813. In 1824 Gerstner [3] conducted tension measurements on steel piano wire and observed ''experiments in which the wire strings revealed sudden yielding.'' Unfortunately, Ger-

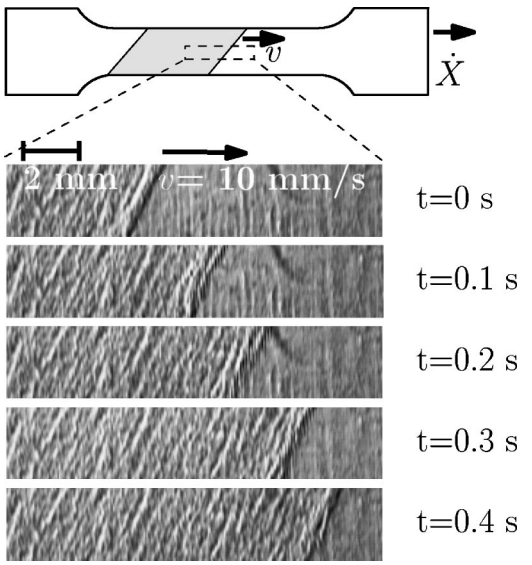

FIG. 1. One end of a dogbone-shaped sample is pulled with speed $\dot{X}$, typically of order 100 μm/s. This results in a front of deformation that moves with speed v of order cm/s. The front leaves behind strained material that is visibly rough.

*Present address: Department of Physics, Rochester Institute of Technology, Rochester, NY 14623.

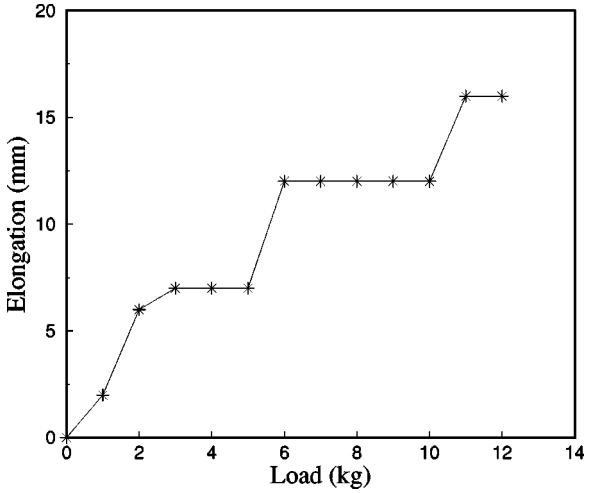

FIG. 2. Masson's observation of temporally inhomogeneous yielding. Note how the sample length remains fixed despite the addition of several kilograms mass before suddenly growing with the addition of a single kilogram. Data from Masson, 1841 [5].

stner goes on to explain that these experiments, the objects of our interest, were ''left out'' of his final discussion.

The true discoverer of the phenomenon is Savart [4], the first to believe that the observed inhomogeneities were a fundamental part of plastic deformation. Savart added weights to the end of copper strips and documented the spatial inhomogeneity now known as Portevin–Le Chatelier bands. Savart assigned the problem to his student, Masson, who in 1841 [5] more carefully controlled the loading rate. Masson observed the strain to remain constant as the load increased until, with only a small change in load, suddenly elongating by several millimeters (see Fig. 2). In his words, ''solid bodies do not elongate in a continuous manner, but by sudden jumps.'' Masson also carefully investigated the effect in different alloys and at different temperatures—the systematic study often ascribed to Portevin and Le Chatelier.

The current attribution may be due to Cottrell, who in 1953 [6] wrote ''The first systematic study of [the phenomenon] was made by Portevin and Le Chatelier in recognition of whom the name 'Portevin–Le Chatelier effect' is now often used.'' Cottrell's attribution has survived despite Bell's [7] attempts to set the record straight.

C. Background

There are many phenomenological discussions of the Portevin–Le Chatelier effect. Their sheer number prohibits a detailed review, but a brief discussion of the common framework within which such theories exist is necessary. Reviews have been provided by Estrin and Kubin [8] and Franklin [9].

One presumption of most theories, which has yet to be checked with care by experiment, is that the dynamics of shear bands can be captured by a one-dimensional description. This reduction is accomplished by averaging the stresses and strains over the shear surface, generally at an angle to the direction of propagation. The strain tensor then collapses to a scalar which varies only along the length of the sample. We have investigated the appropriateness of this simplification and it appears to be valid in the case of steadily moving fronts.

The deformation is described by the total strain, $\epsilon_{\mathrm{tot}} = \partial u/\partial x$, which is the sum of the elastic strain ϵ_e and the plastic strain ϵ_p. The elastic strain is completely reversible and linearly related by Young's modulus E to the applied stress σ according to Hooke's Law,

$$\sigma = E\epsilon_e . \tag{1}$$

The plastic strain is irreversible and occurs whenever a load is applied. Straining at low stresses is exponentially small and called creep. The stress at which appreciable straining begins is known as the flow stress σ_f. The flow stress increases as a sample strains, i.e., the sample hardens as it strains. This is called work hardening, and in many cases the flow stress increases roughly as the square root of ϵ_p. One mechanism for work hardening is the increased entanglement of dislocations which require ever-larger stresses in order to break free.

The flow stress also depends upon the rate at which the sample is deformed, revealing an interaction between dislocation motion and other time scales (e.g., diffusion of impurity atoms) inside the metal. The rate dependence, called the strain-rate sensitivity, is not as well defined; experiments investigating this behavior are described below. It is common [10–12] to assume that the plastic strain rate $\dot{\epsilon}_p$ depends exponentially on the difference between the applied stress σ and the flow stress $\sigma_f(\epsilon_p, \dot{\epsilon}_p)$

$$\dot{\epsilon}_p \propto \frac{1}{\tau_1} \exp\left[\frac{\sigma - \sigma_f(\epsilon_p, \dot{\epsilon}_p)}{E}\right], \tag{2}$$

where τ_1 is a time constant. For a given stress σ, Eq. (2) describes a constitutive relation that the strain rate $\dot{\epsilon}$ satisfies. In the simplified case of a one-dimensional system, the applied stress σ is uniform, determined by the boundary conditions imposed on the sample.

D. Strain-rate sensitivity: Homogeneous vs inhomogeneous yielding

Phenomenological descriptions of the Portevin–Le Chatelier effect have centered on the rate dependence of the flow stress σ_f. Penning [13] showed that homogeneous deformation is unstable when the flow stress decreases with increasing strain rate. This behavior is referred to as negative strain-rate sensitivity. While this mechanism does produce an instability, and produces a serrated stress-strain curve similar to that observed in the laboratory, the spatial behavior is not of the form of propagating fronts [17]. The instability grows fastest at short wavelengths and is unphysical. In subsequent work various diffusion terms were added to the flow stress [18] but these also fail to reproduce even qualitatively front dynamics [19].

The rate dependence of the flow stress is not known with certainty because interpretation of experiments designed to investigate it is difficult. There is a natural tendency to use results from homogeneously deforming samples in the constitutive equation [Eq. (2)] to explain the Portevin–Le Chatelier effect. For example, experiments to probe the rate dependence of the flow stress (described below) measure the stresses required to maintain various global strain rates. The stress dependence on global strain-rate rates is then incorporated into constitutive equations as critical *local* strain rates.

But the physics governing the Portevin–Le Chatelier effect necessarily localizes the deformation. It is not at all obvious that the local stresses and strain rates experienced during inhomogeneous yielding are similar to those measured in homogeneous deformation. Negative strain-rate sensitivity can therefore be understood in the case of homogeneous deformation, but its role in localized yielding is unclear. Our experiments, for example, do not show a negative strain-rate sensitivity and this behavior is captured in our model.

Experimental study of negative strain-rate sensitivity has taken two different forms. Bodner and Rosen [14,15] imposed a constant pulling speed and measured the stress necessary to reach a given strain. They found that less stress was needed to reach a given strain at higher pulling speeds. Bodner and Rosen's data show no serrations, which seems to indicate their samples are deforming homogeneously. Later experiments by van den Brink [10] and Ling [16] subjected a homogeneously deforming sample to a sudden change in pulling speed. The strain-rate sensitivity $\Delta\sigma/\Delta\dot{\epsilon}_p$ was obtained by measuring the change in stress $\Delta\sigma$ that accompanied a change in strain rate $\Delta\dot{\epsilon}_p$. For a range of strains and strain rates the stress fell below its original value. The interpretation was that a lower stress was required to deform the material at the higher rate. For low strains the strain-rate sensitivity was positive, consistent (it was thought) with the observation that the serrations occur only after an initial, homogeneous deformation. It is important to note that both Bodner and Rosen and van den Brink's experiments are restricted to homogeneously deforming samples. In our theoretical framework, negative strain-rate sensitivity can *only* be observed in a homogeneously deforming sample, and is a direct consequence of the nonlinear flow stress relation $\sigma_f(\epsilon_p)$.

II. THEORY

A. Constraints on phenomenology

A successful phenomenology of the Portevin–Le Chatelier effect must reproduce the following observations: (1) deformation fronts exist and move in steady fashion at velocities much slower than the speed of sound c, (2) at very low deformation rates fronts cease to move continuously, and (3) once a front has propagated throughout the sample, another can be initiated if the stress is increased. Subsequent fronts move more slowly but are qualitatively identical to their predecessors.

We have found that almost all features of deformation—both homogeneous and inhomogeneous—can be reproduced by assuming that the flow stress depends not on the customary local strain rate but rather on a nonlocal strain rate $\tilde{\dot{\epsilon}}$, defined as

$$\tilde{\dot{\epsilon}} = G(x,t) * \dot{\epsilon} \tag{3}$$

$$\equiv \int G(x',t')\,\dot{\epsilon}_p(x-x',t-t')\,dx'\,dt'. \tag{4}$$

The idea is that deformation at a given point depends on deformation in neighboring regions in some way linear in $\dot{\epsilon}_p$. Equation (4) is the most general way of expressing dependence. The function G smears the local strain-rate $\dot{\epsilon}_p$ over a characteristic length l and time τ_2. Constitutive relations involving convolutions as in Eq. (4) are standard in the electromagnetic response of dielectric media and in the mechanical behavior of polymeric fluids. While a possible physical motivation for such a term may be found in the various mechanisms for dislocation creation, we do not pursue this too strongly. The theory is a phenomenological one.

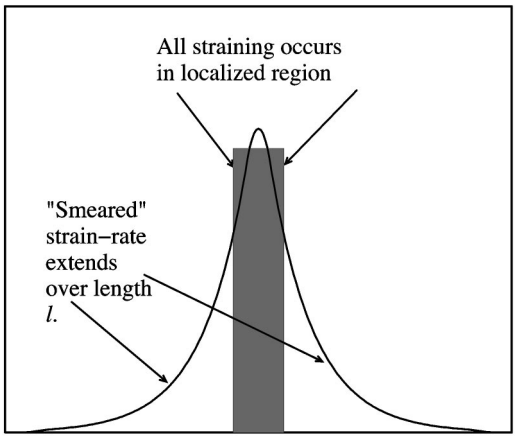

FIG. 3. The relation between the local strain rate $\dot{\epsilon}_p$ and the ''smeared'' strain-rate $\tilde{\dot{\epsilon}}$. All plastic straining is confined to within the shaded region but $\tilde{\dot{\epsilon}}$ extends outside of this region as indicated by the solid line.

While there is no direct connection with dislocations, we think of $\dot{\epsilon}$ as representing an active dislocation population spawned in a region surrounding areas of plastic deformation. They remain active for some characteristic time governed by the time decay rate of $G(x,t)$, and then become pinned.

The spatial relation between $\tilde{\dot{\epsilon}}$ and $\dot{\epsilon}_p$ is shown in Fig. 3. The strain rate $\dot{\epsilon}_p$ is localized within the filled rectangle. The resulting smeared strain rate $\tilde{\dot{\epsilon}}$ is shown by the solid line. We propose that it is the nonlocal strain rate that is responsible for reducing the flow stress. Thus in Fig. 3 the deforming material weakens the adjacent material. This process continues until the adjacent material is sufficiently weakened that the deformation spreads. The kernel G is also time dependent, so the effects of deformation on flow stress are delayed by a characteristic time that we identify tentatively as an empirical diffusion time.

A sketch of the flow stress as a function of nonlocal strain rate is shown in Fig. 4. The flow stress decreases with increasing $\tilde{\dot{\epsilon}}$, becoming constant at higher rates as the weakening effect saturates. If the stress is below the minimum flow stress (75 MPa in Fig. 4) no deformation occurs; stresses above the maximum flow stress (90 MPa) cause deformation everywhere simultaneously. If the stress is at an intermediate value, however, the sample deforms inhomogeneously. Places where $\tilde{\dot{\epsilon}}$ is large enough to appreciably weaken the material deform while portions where $\tilde{\dot{\epsilon}}$ is small do not.

B. Equations

1. Constitutive equation for strain

Flow below the flow stress, called creep, is exponentially small and not a crucial component of the Portevin–Le Chat-

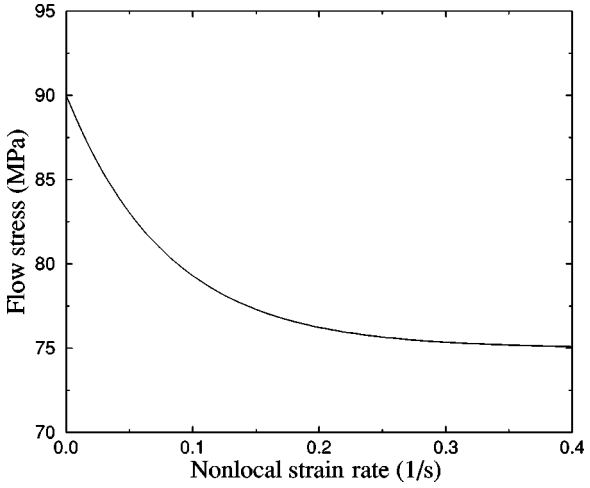

FIG. 4. Flow stress as a function of nonlocal strain rate $\tilde{\dot{\epsilon}}$.

elier effect. We simplify the analysis by ignoring creep, and also assume that the plastic strain rate $\dot{\epsilon}_p$ is proportional to the difference between the stress σ and the flow stress σ_f, made dimensionless by dividing through by Young's modulus E

$$\frac{\partial \epsilon_p(x,t)}{\partial t} = \begin{cases} cl\,\dfrac{\sigma(t)-\sigma_f(x,t)}{\tau_1} & \text{whenever} \quad \sigma > \sigma_f(\epsilon_p, \tilde{\dot{\epsilon}}) \\ 0 \quad \text{whenever} \quad \sigma < \sigma_f(\epsilon_p, \tilde{\dot{\epsilon}}). \end{cases} \tag{5}$$

The flow stress σ_f depends upon both the strain ϵ_p and the nonlocal strain rate $\tilde{\dot{\epsilon}}$, and varies across the sample.

In constructing the theory we also assume that the experiments are effectively one-dimensional. This implies that the stress is constant throughout the length of the sample and that necking is negligible as pertains to front propagation. This must be checked experimentally, and in fact the magnitude of necking is comparable to that of some of the observables. Why do we feel justified in ignoring necking? We must find appropriate coupling terms to generate front propagation. Diffusion is the customary mechanism, and terms to account for necking take the same form as diffusion. That is, terms that express the local three-dimensional (3D) effect of necking as one-dimensional (1D) nonlocal terms are diffusional. We have unambiguously shown, however, that diffusion terms do not lead to propagating fronts at a constant stress. Although necking is clearly present, and perhaps significant, we conclude that something else must be responsible for the front propagation.

For $G(x,t)$ we choose

$$G(x,t) = \frac{1}{2l\tau_2} e^{-|x|/l} e^{-t/\tau_2}. \tag{6}$$

Equation (4) (the definition of $\tilde{\dot{\epsilon}}$) is then formally equivalent to the following differential equation:

$$\frac{\partial \tilde{\dot{\epsilon}}(x,t)}{\partial t} = \frac{1}{2l\tau_2}\int_0^L dx'\,\dot{\epsilon}_p(x',t) e^{\frac{-|x-x'|}{l}} - \frac{\tilde{\dot{\epsilon}}(x,t)}{\tau_2}. \tag{7}$$

Equation (7) indicates that the nonlocal strain rate $\tilde{\dot{\epsilon}}$ at a point is produced by any straining within a distance l and decays over the characteristic time τ_2. Our results are insensitive to the particular form of $G(x,t)$. Replacing $\exp[-|x|/l]$ by $\exp[-x^2/l^2]$, for example, does not change the results appreciably. The particular form in Eq. (7) is convenient for analytical work.

2. Boundary conditions

The relevant boundary conditions for both experiment and theory are

$$v(x=0)=0, v(x=L)=\dot{X}. \tag{8}$$

These determine the stress throughout the sample for our one-dimensional model, which is simply proportional to the elastic part of the deformation and is expressed mathematically by the machine condition

$$\sigma(t) = \mu\left[X(t) - \int_0^L dx'\,\epsilon_p(x',t)\right]. \tag{9}$$

$X(t)$ is the machine displacement, and the integral is the total plastic strain throughout the sample; Eq. (9) is essentially Hooke's law, and μ is an effective spring constant that characterizes the testing machine. It depends upon the sample length L and cross-sectional area A, Young's modulus E, and the stiffness of the machine K as

$$\mu = \frac{KE}{KL+EA}. \tag{10}$$

An infinitely soft machine has a μ equal to zero while an infinitely hard machine has a μ of E/L.

For any particular testing machine μ can be determined from the stress-strain curve prior to the onset of plastic deformation. All deformation is elastic and Eq. (9) reduces to $\sigma = \mu X(t)$. The stress increases linearly with the extension (Hooke's law) with a slope μ. The machine used in our experimental tests has

$$\mu = 432\,000 \ \text{MPa/m}. \tag{11}$$

The ratio of our machine μ to the theoretical maximum is (with a 10 cm sample)

$$\frac{\mu}{\mu_\infty} = 0.6. \tag{12}$$

Our machine can be characterized as moderately stiff, corresponding to a simple spring with a spring constant of approximately $K = 1.4\times 10^7$ N/m.

3. Flow stress

The flow stress $\sigma_f(\epsilon_p, \tilde{\dot{\epsilon}})$ is defined as the stress at which appreciable plastic deformation begins. It depends on both plastic strain ϵ_p and nonlocal strain rate $\tilde{\dot{\epsilon}}$ and we assume this dependence is separable,

$$\sigma_f(\epsilon_p, \tilde{\dot{\epsilon}}) = \Upsilon(\epsilon_p) f(\tilde{\dot{\epsilon}}). \tag{13}$$

As discussed earlier, Bodner and Rosen [14,15] measured the flow stress at different end velocities; their data are consistent with the separation in Eq. (13). Curves for different end velocities are qualitatively similar and are well approximated (at constant end velocity) by a square-root function

$$\sigma_f(\epsilon) = \sigma_y \sqrt{\epsilon_p}, \tag{14}$$

with σ_y a property of the material. Sharpe [20] quotes $\sigma_y = 384$ MPa for aluminum.

In our experiments we are careful always to initiate fronts at the same value of plastic strain. Later we will generalize our equations to account for multiple fronts. Successive fronts occur after the previous front has passed completely through the sample. We therefore separate the strain due to any existing fronts ϵ_p from all other plastic strain, which we label ϵ_y. ϵ_y includes any strain introduced during sample preparation, such as rolling or machining, as well as deformation introduced during testing prior to the appearance of the front. The flow stress can then be written as

$$\sigma_f(\epsilon_p, \tilde{\dot{\epsilon}}) = \sigma_y \sqrt{\epsilon_y + \epsilon_p} f(\tilde{\dot{\epsilon}}). \tag{15}$$

The strain from the front ϵ_p typically is smaller than ϵ_y, the strain at initiation. For the purposes of a single front we expand Eq. (15) about $\epsilon_p = 0$ to get

$$\sigma_f(\epsilon, \tilde{\dot{\epsilon}}) = \sigma_y \sqrt{\epsilon_y} \left(1 + \frac{\epsilon_p}{2\epsilon_y}\right) f(\tilde{\dot{\epsilon}}). \tag{16}$$

The central nonlinearity responsible for inhomogeneous yielding is contained in the function $f(\tilde{\dot{\epsilon}})$. Experiments on homogeneously deforming samples indicate that the flow stress drops with strain rate. We propose that the details of the functional form of this drop are not important. In our analytical work we use the discontinuous function

$$f(\tilde{\dot{\epsilon}}) = 1 - \lambda\, \theta(\tilde{\dot{\epsilon}} - \tilde{\dot{\epsilon}}_c), \tag{17}$$

which drops suddenly when the nonlocal strain rate $\tilde{\dot{\epsilon}}$ surpasses a critical value $\tilde{\dot{\epsilon}}_c$.

Our results are qualitatively independent of the specific nature of $f(\tilde{\dot{\epsilon}})$. What is essential is that f is a function of the nonlocal strain rate $\tilde{\dot{\epsilon}}$, rather than the local strain rate $\dot{\epsilon}_p$. $\tilde{\dot{\epsilon}}$ and $\dot{\epsilon}_p$ are identical for homogeneous and steady deformation so data from such experiments can be used to determine the particular nature of $f(\tilde{\dot{\epsilon}})$. Figure 5 shows front profiles from simulations using three different functions for $f(\tilde{\dot{\epsilon}})$: the step function used in the analytics, a piece wise linear function, and an exponential decay from 1 to λ. The profiles in Fig. 5 have been normalized by the final strain to emphasize the qualitative similarity in shape. This makes sense on physical grounds, since the width of the front is quite small the system actually spends very little time between the extreme values. Front characteristics are determined by the initial and final value of the strain and not on how the system passes from one to the other.

Choosing Eqs. (16) and (17) makes possible the analytic integration of the equation for the plastic strain [Eq. (5)].

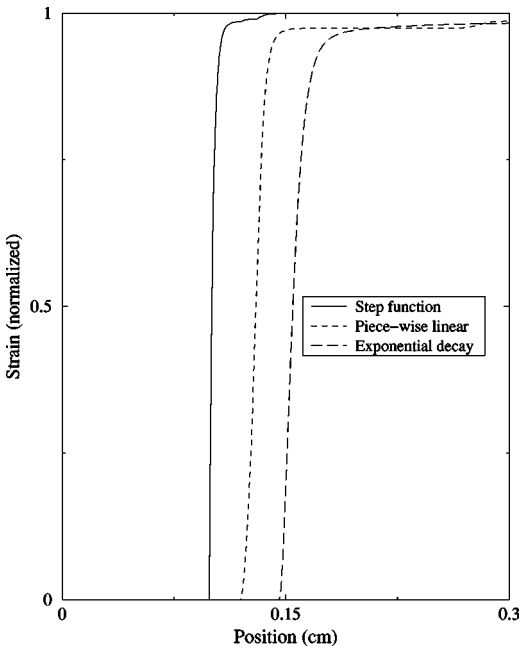

FIG. 5. Strain profiles from three simulations, each using a different function for $f(\tilde{\dot{\epsilon}})$. Strains have been normalized by the maximum strain to emphasize similarities in profile. The solid line results from use of a step function and results in the steepest profile. The dashed line is the profile resulting from a piece-wise linear function while the long-dashed line is that of a continuous, exponentially decay. The qualitative similarity between all three fronts indicates the independence of our results from specific function used for $f(\tilde{\dot{\epsilon}})$.

Numerical solutions with different forms of the flow stress, including differentiable functions, produce no qualitative difference.

C. Solving the steady-state equations

When the initial conditions include inhomogeneities, numerical solution of Eqs. (5)–(7) reveals fronts that propagate at constant stress at speeds of centimeters per second [1]. The prediction of propagation at constant stress contradicts the common view that fronts propagate only under increasing stress. This prediction has been confirmed by our experiments. We now describe in more detail the motion of steady fronts. The solution permits close quantitative comparison between theory and experiment.

We first move to a coordinate system traveling with constant velocity v. The origin is taken to be the point where the stress first equals or exceeds the flow stress; the strain rate is thus zero for x less than zero. The background strain ϵ_y is constant throughout the sample while strain produced by the front ϵ_p increases from zero. The definition of the origin as the point where straining first occurs implies that there the stress equals the flow stress

$$\sigma = \sigma_f(x=0) = \sigma_y \sqrt{\epsilon_y} f(\tilde{\dot{\epsilon}}(0)). \tag{18}$$

According to Eq. (17), $f(\tilde{\dot{\epsilon}})$ is less than one only when $\tilde{\dot{\epsilon}} \geqslant \tilde{\dot{\epsilon}}_c$; this fixes the value of the nonlocal strain rate at the origin to the critical value $\tilde{\dot{\epsilon}}_c$

$$\tilde{\dot{\epsilon}}(x=0)\equiv\tilde{\dot{\epsilon}}_c. \tag{19}$$

At the origin the flow stress discontinuously drops and the plastic strain-rate abruptly becomes nonzero.

In steady state the evolution equation for the strain is

$$v\frac{d\epsilon_p(x)}{dx}=\frac{\sigma-\sigma_f(\epsilon_p,\tilde{\dot{\epsilon}}_c)}{\tau_1}\,(x>0) \tag{20}$$

and the equation for the nonlocal strain rate Eq. (7) is

$$v\frac{d\tilde{\dot{\epsilon}}(x)}{dx}=\frac{1}{2l\tau_2}\int_0^L dx'\,v\frac{d\epsilon_p(x')}{dx'}e^{(-|x-x'|)/l}-\frac{\tilde{\dot{\epsilon}}(x)}{\tau_2}. \tag{21}$$

These equations are subject to the following conditions:

$$\epsilon_p(x\leqslant 0)=0,\tilde{\dot{\epsilon}}(\pm\infty)=0,\tilde{\dot{\epsilon}}(0)=\tilde{\dot{\epsilon}}_c. \tag{22}$$

Equation (20) incorporates one further approximation. At the tail end of a front $\tilde{\dot{\epsilon}}$ dips below $\tilde{\dot{\epsilon}}_c$, and all motion locks up instantly. We continue to use Eq. (20) in this region; deformation is dropping exponentially quickly to zero anyway, and it is much simpler to have only one boundary at the origin, where the strain rate discontinuously changes, rather than two. The consequences of this simplification will be seen to be minor.

To find the strain, Eq. (20) is integrated subject to the following conditions:

$$\epsilon_p(0)=0,\epsilon_p(\infty)=\delta\epsilon(\sigma), \tag{23}$$

the strain exponentially approaches a constant as

$$\epsilon_p(x>0)=\delta\epsilon(\sigma)\left(1-\exp\left[\frac{-\sigma_y}{2v\tau_1\sqrt{\epsilon_y}}\,x\right]\right). \tag{24}$$

We can solve for the strain jump across the front $\delta\epsilon$ since straining stops when strain hardening has increased the flow stress to once again surpass the applied stress

$$\sigma=\sigma_y\sqrt{\epsilon_y}\left(1+\frac{\delta\epsilon}{2\epsilon_y}\right)(1-\lambda) \tag{25}$$

$$\Rightarrow\delta\epsilon(\sigma)=2\epsilon_y\left[\frac{\sigma}{\sigma_y\sqrt{\epsilon_y}}-(1-\lambda)\right]. \tag{26}$$

The strain jump $\delta\epsilon$ depends upon the stress σ and strain at onset ϵ_y, and thus changes for successive fronts.

For a constant pulling speed $\dot{X}$ we observe fronts that travel with a constant velocity v. The machine condition Eq. (9) then requires that

$$\dot{X}=v\,\delta\epsilon(\sigma), \tag{27}$$

where the strain jump $\delta\epsilon(\sigma)$ is a function of the stress. This provides one equation for two unknowns (stress σ and front velocity v). Equation (27) also includes the only independent variable from the experiment (the pulling speed).

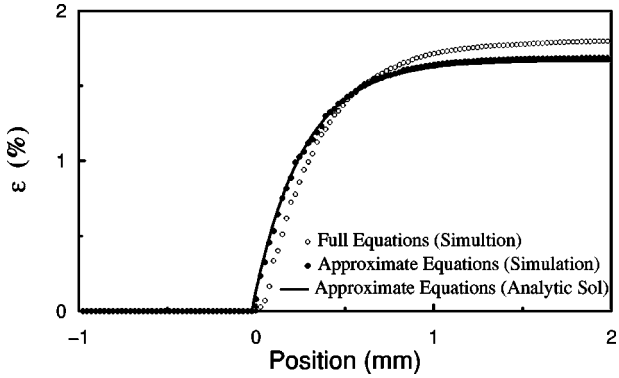

FIG. 6. Strain profiles from simulations of the approximate (●) and full (○) equations compared with the analytic solution (solid line) of the approximate equations. The differences between the simulation of the full equations and the analytic solution are slight. We can therefore apply results from the analytic solution to the real system.

The solution for the strain Eq. (24) is used to integrate Eq. (21) to solve for $\tilde{\dot{\epsilon}}(x)$ for x less than zero. The result is that $\tilde{\dot{\epsilon}}(x)$ decays exponentially to zero as one moves away from the origin,

$$\tilde{\dot{\epsilon}}(x<0)=A_0(\sigma,v)\exp\left[\frac{x}{l}\right]. \tag{28}$$

The rate of decay depends only upon the parameter l. As this parameter governs the spatial smearing of $\dot{\epsilon}_p$ its appearance here is quite logical. The coefficient of the exponential depends on the stress σ and front velocity v,

$$A_0(\sigma,v)=\frac{\sigma_y\delta\epsilon(\sigma)}{4\tau_1\tau_2\sqrt{\epsilon_y}\left(\frac{v}{l}+\frac{1}{\tau_2}\right)\left(1+\frac{\sigma_y l}{2v\tau_1\sqrt{\epsilon_y}}\right)}. \tag{29}$$

Requiring $\tilde{\dot{\epsilon}}=\tilde{\dot{\epsilon}}_c$ at the origin produces the second relation between stress and front velocity,

$$A_0(\sigma,v)=\tilde{\dot{\epsilon}}_c. \tag{30}$$

Equations (27) and (30) determine a unique stress and front velocity that result from an imposed pulling speed.

It is possible to solve Eq. (21) for x greater than zero; $\tilde{\dot{\epsilon}}$ is a sum of exponentials

$$\tilde{\dot{\epsilon}}(x>0)=A_1\exp\left[\frac{-x}{l}\right]+A_2\exp\left[\frac{-x}{v\tau_2}\right]+A_3\exp\left[\frac{-\sigma_y}{2v\tau_1\sqrt{\epsilon_y}}\right]. \tag{31}$$

A_1, A_2, and A_3 are complicated functions of σ and v. The nonlocal strain rate is continuous across the origin and so $A_1+A_2+A_3=A_0$. Since a minor approximation was employed in this analysis, it is wise to compare the results with direct numerical solution. Figure 6 shows the strain profile of three fronts. The solid line is the analytic solution. It matches exactly the profile from a numeric simulation of the approximate equations, shown as the solid dots. The open circles are the result of simulations of the full, nonapproximate, equa-

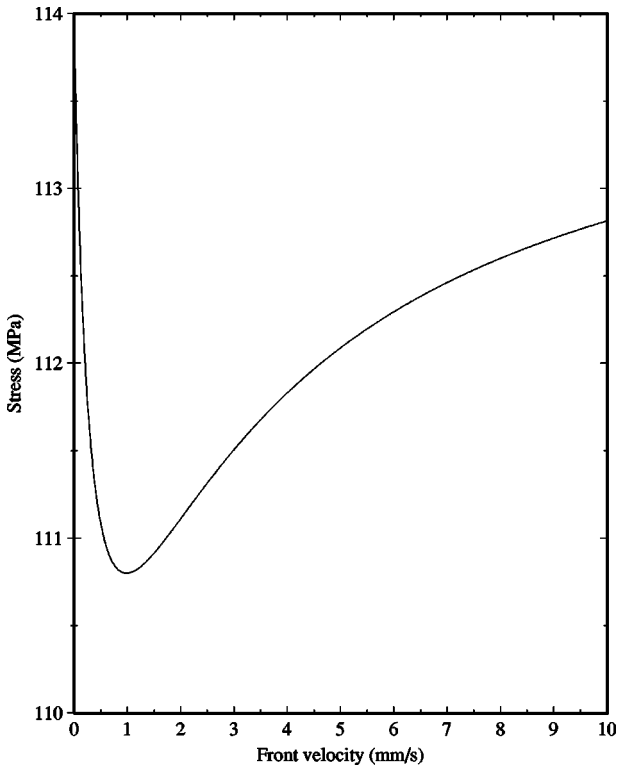

FIG. 7. Theoretical flow stress as a function of front velocity. The descending portion of the curve is unstable; perturbations to a steady front grow via a mechanism similar to that of ordinary frictional stick-slip motion.

tions. Note the slightly larger final strain ($\sim 8\%$) realized in the full equations, a consequence of the approximations discussed above. Note also the practical width of the front (1 mm) and strain jump (1.5%), both in accord with experiment.

D. Stability

The stability of the traveling front solution can be most easily determined by examining how the flow stress depends upon the front velocity. This is shown in Fig. 7. The descending part of the curve in Fig. 7 marks a region in which the steady-state solution is unstable. The mechanism for this instability is similar to that found in ordinary stick-slip friction and brittle fracture. A small perturbation that increases the front speed lowers the flow stress, accelerating the front. Similarly, a perturbation that slows the front speed results in a larger flow stress, further slowing the front. Numerical simulations confirm this picture. An end velocity that corresponds to a front speed in the unstable region does not result in a front moving at constant speed. Rather the front moves in erratically, alternating periods of motion and rest.

This behavior is also seen in the experiments. At low pulling speeds fronts do not move throughout the sample with constant velocity. Rather the front appears to hop; elastic straining is followed by a brief burst of plastic straining. During the plastic strain, the front moves a distance of order of the sample thickness before again coming to rest [21]. The pulling speed at which fronts begin to move continuously is easily determined experimentally and is one of the observations we use to determine values for our parameters.

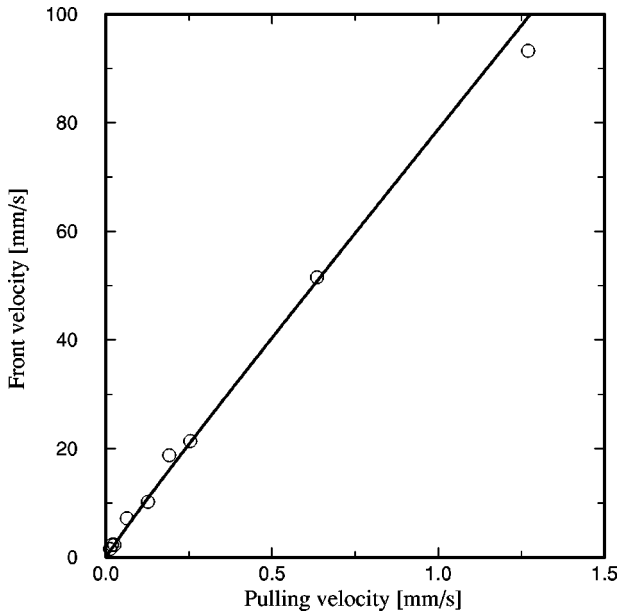

FIG. 8. Front velocity for continuously moving fronts as a function of pulling speed. The linear relation is consistent with our theory and used to determine the parameter λ.

III. RESULTS

The main weakness of the phenomenology we have developed is its dependence on five parameters, τ_1, τ_2, l, $\tilde{\epsilon}$, and λ. To give the theory predictive power they must be related as directly as possible to specific experiments, and then remain locked in value and compared with different experiments. We now describe the measurements needed to fix the parameters. This also highlights the theory's qualitative predictions that are confirmed by experiment.

A. Velocity selection

The theory predicts that the velocity of a front is simply proportional to the pulling speed, a fact observed in previous experiments. The proportionality constant uniquely determines the parameter λ of the model. The strain jump across the front is

$$\delta\epsilon(\sigma) = 2\epsilon_y\left[\frac{\sigma}{\sigma_y\sqrt{\epsilon_y}} - (1-\lambda)\right] \tag{32}$$

which, since the stress is always within a few percent of the upper yield stress $\sigma_y\sqrt{\epsilon_y}$, is to good approximation

$$\delta\epsilon = 2\epsilon_y\lambda. \tag{33}$$

The strain jump depends only on the strain at initiation and the parameter λ. We have confirmed with experiments [1] that the strain jump is independent of pulling speed. The relation between front velocity and pulling speed Eq. (27) becomes

$$v = \frac{1}{2\epsilon_y\lambda}\dot{X}. \tag{34}$$

A comparison between the experimental observations and the theoretical prediction is shown in Fig. 8. A linear fit to the data results in a value of

$$\lambda = 0.175. \tag{35}$$

Should a second front follow the first it will introduce a larger strain jump [since ϵ_y is larger in Eq. (33)] and travel more slowly than its predecessors [Eq. (34)]. This has not yet been investigated experimentally for continuously moving fronts.

B. Exponential decay of stress upon yielding

The onset of plastic yielding is accompanied by a sharp decrease in the stress as the sample ''catches up'' to the machine. This is seen in both theory and experiment regardless of whether the fronts hop or move continuously. The following calculation shows that the model predicts this decay to be exponential, and the rate of decay uniquely determines the parameter τ_1.

If all of the plastic straining takes place within a narrow band of width w then the total rate of plastic deformation can be replaced expressed as $\overline{\dot{\epsilon}_p} w$, where $\overline{\dot{\epsilon}_p}$ is the average strain rate in the band. Differentiating the machine condition with respect to time gives

$$\frac{d\sigma}{dt} = \mu(\dot{X} - w\overline{\dot{\epsilon}_p}) \approx \mu\left(\dot{X} - w\frac{\sigma - \sigma_f}{\tau_1}\right). \tag{36}$$

The last relation was obtained by using Eq. (5) to define the strain rate in terms of the stress and flow stress. If the stress decay occurs quickly, changes in the strain, and hence the flow stress, are negligible. Equation (36) is a differential equation for the stress as a function of time with all other quantities constant. The solution of this equation is (introducing the integration constant Σ)

$$\sigma(t) = \left(\frac{\dot{X}\tau_1}{w} + \sigma_f\right) + \Sigma \exp\left[\frac{-\mu w}{\tau_1} t\right]. \tag{37}$$

The stress decay is exponential with the steepness of the decay depending only upon the stiffness of the machine, the width of the front, and the time constant τ_1. Determination of the machine stiffness μ has been described above and the front width w can easily be obtained from video images. The width is approximately equal to the sample thickness, 1 mm. The slope of a logarithmic linear plot of $\sigma(t)$ vs t then determines τ_1. This plot is shown in Fig. 9; the slope gives a value of $\tau_1 = 1.2 \times 10^{-3}$ s. τ_1 is the parameter that governs how quickly the sample responds to changes in the stress; it is thus natural that it also governs the transient behavior of the stress.

C. Stress at which fronts travel

A fundamentally new prediction of the theory is that deformation fronts travel at constant stress. Experimental confirmation of this, as reported in [1], casts doubt on other theories that predict fronts to progress only under an increasing stress.

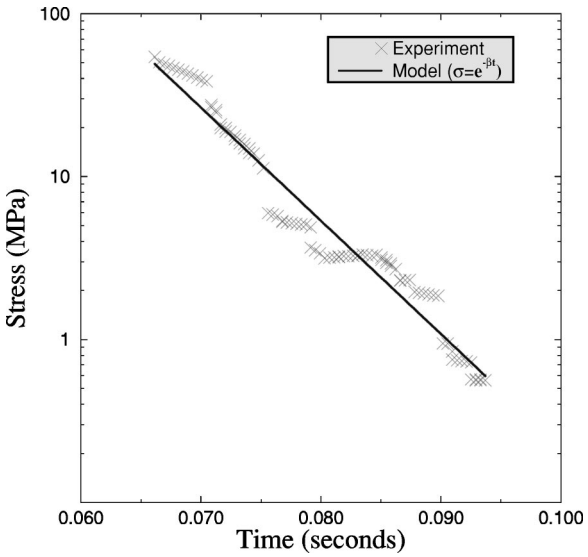

FIG. 9. Initial yielding of a sample is predicted to be exponential. This is seen in the experiment ($\times$) and is used to fix the parameter τ_1 in the model.

The remaining three parameters are determined by two separate experiments. It has been previously observed [22,1] that at low pulling speeds the fronts hop rather than move steadily. At low pulling speeds steadily moving fronts are unstable, and thus physically unrealizable. The minimum speed at which steady fronts are stable is

$$\dot{X}_{\min} = \lambda l \epsilon_y \sqrt{\frac{2\sigma_y}{\tau_1 \tau_2 \sqrt{\epsilon_y}}}. \tag{38}$$

Experiments indicate a minimum pulling speed of 13 μm/s, or a front speed of 1.2 mm/s; this is used to express τ_2 as a function of l,

$$\tau_2 = \frac{\sigma_y}{2\tau_1 \sqrt{\epsilon_y} (1.2 \times 10^{-3})^2} l^2. \tag{39}$$

The set of independent parameters has thus been reduced to two: $\tilde{\dot{\epsilon}}_c$, the critical value of the nonlocal strain rate at which weakening commences and l, the distance over which the strain rate is smeared. The stress at two different pulling speeds are used to fix these parameters. We choose the stress corresponding to the slowest possible front, i.e., the transition velocity, and the stress at the fastest observed front. The former is 1108 newton, the latter (at a pulling speed of 1300 μm/s) is 1130 newton. Fitting the parameters $\tilde{\dot{\epsilon}}_c$ and l to these two points gives

$$l = 50 \ \ \mu\text{m}, \quad \tilde{\dot{\epsilon}}_c = 0.027 \ \ \text{s}^{-1}, \quad \tau_2 = 0.04 \ \ \text{s}. \tag{40}$$

The experimental error for these measurements is about 2%. Our parameters are fairly sensitive to this uncertainty. Holding four parameters constant, the fifth changes by as much as 20% to accommodate this.

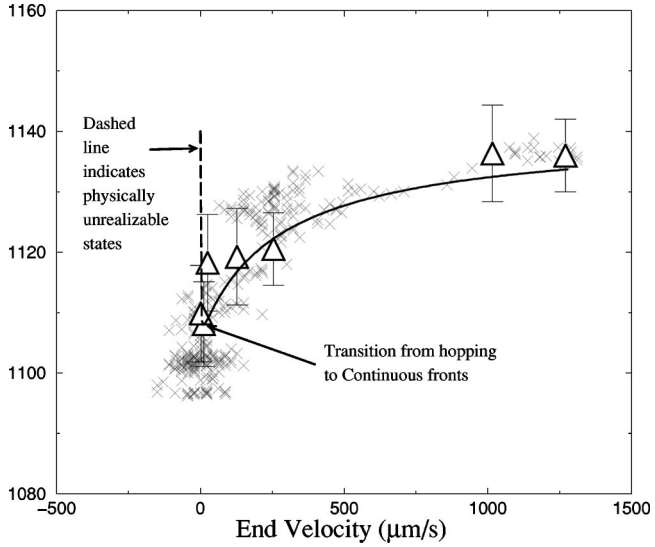

FIG. 10. Theoretical prediction for stress as a function of the end velocity compared with experimental observation. The dashed line indicates the region of unrealizable steady fronts; in this region hopping fronts occur in both simulation and experiment.

IV. COMPARING THEORY AND EXPERIMENT

A. Constant pulling-speed experiments

With the parameters fixed, we can compare the stress predicted by the theory with that measured in the laboratory at different pulling speeds. Solving Eqs. (27) and (30) produces a functional relation between the stress and pulling speed; the resulting curve is shown in Fig. 10. Results from six different experiments are shown as △'s and the theoretical prediction (solid line) passes through all six, within experimental error. The ×'s are from experiments where the pulling speed changes; in this case the experiment sweeps through a range of pulling speeds. The theoretical curve nicely follows the experimental results.

B. The transition to hopping fronts

The solid line in Fig. 10 is the theoretical solution for the steady-state load as a function of pulling speed. As the pulling speed increases from zero, the stress drops from the maximum flow stress $\sigma_y\sqrt{\epsilon_y}$. The curve has a well-defined minimum, after which it asymptotically approaches the maximum flow stress from below. As mentioned earlier, solutions in the descending region of the curve are numerically unstable and thus physically unrealizable. This is marked in Figure 10 by a dashed line. Numerical simulations show that in this region fronts do not move steadily. Instead the front alternates appreciable periods of rest (in which the stress steadily increases) with sudden, short periods of motion. This is similar to the hopping fronts observed in prior experiments [22,1]. The mechanism for this instability is similar to that which causes stick-slip motion in simple friction experiments.

C. ''Double-ramp'' experiments

The quantitative agreement of theory and experiment is nicely illustrated in an experiment in which the pulling speed is abruptly changed. Fig. 11 shows this comparison. The ●'s

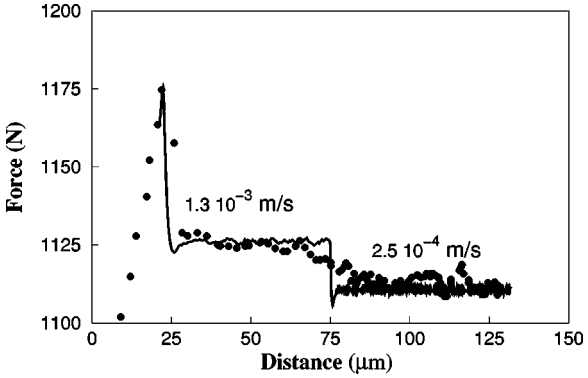

FIG. 11. The change in stress accompanying a sudden change in pulling speed. Theory (solid line) and experiment (●) agree quite well in all phases of the curve.

are experimental data and the solid line the result of numerical simulations. Note the qualitative agreement in all stages of the curve: the elastic loading, the initial yield to the lower stress level, and the smooth increase to the new stress. The largest difference is in the transition that accompanies the change in pulling speed. Although the loading machine is programmed to change speeds quickly, the actual acceleration depends on the sample response to sudden changes in stress. This response is complicated and not known. The simulation does change speed instantaneously, resulting in the sharp transition of Fig. 11.

D. Homogeneous yielding and negative strain-rate sensitivity

As described in Sec. I, experimental observations of negative strain rate sensitivity have involved homogeneously deforming samples. When deformation is homogeneous the nonlocal strain rate $\tilde{\dot{\epsilon}}$ reduces to the local strain rate ϵ_p

$$\tilde{\dot{\epsilon}}=\dot{\epsilon}_p, \tag{41}$$

and the flow stress is the traditional function of the local strain rate.

For a homogeneously deforming sample there is a steady-state solution to Eqs. (5)–(7) in which the strain grows linearly with time

$$\epsilon_p=\frac{\mu\dot{X}}{\mu L+\dfrac{\sigma_y}{2\sqrt{\epsilon_y}}}t. \tag{42}$$

Negative strain rate sensitivity occurs when the sudden increase in pulling speed increases the strain rate, lowering the flow stress. The sample flows more quickly and the stress falls. In a simulation with the same parameter set derived above the end velocity was abruptly changed from 100 μm/s to 1000 μm/s after 1 s of smooth straining. The stress transient that accompanies this change is shown in Fig. 12.

The dashed line in Fig. 12 indicates the stress that would accompany a constant end velocity test. Increasing the end velocity causes a stress transient that falls below the steady-state stress associated with the slower end velocity. The increased slope of the stress-time curve after the transient corresponds to the larger steady-state strain rate. Transients

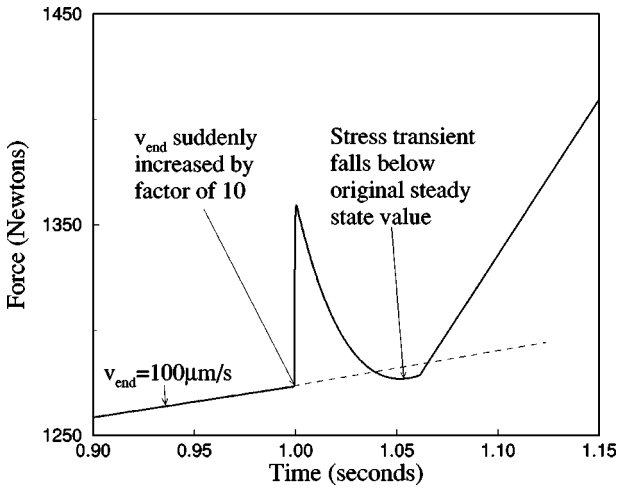

FIG. 12. Simulation of a homogeneous sample subjected to an abrupt change in strain rate (end velocity). At $t=1$ s the pulling speed is increased from 100 μm/s to 1000 μm/s.

qualitatively identical to this were observed in experiments by van den Brink [10] on homogeneously deforming samples and were identified as indicating negative strain-rate sensitivity.

van den Brink also observed that at low strains the transients did not fall below the original stress. It was only at larger strains that the transients dipped below the original stress. Figure 13 shows the results of three simulations, at different strains, in which the pulling speed was abruptly increased. At low strains the sudden change in pulling speed results in an increase of the stress, i.e., positive strain-rate sensitivity. This changes at higher strains with the stress ultimately falling below the original level. The strain dependence is due to the square-root dependence of flow stress on strain. As the strain increases, $\partial\sigma_f/\partial\epsilon$ decreases, and so more strain is necessary to increase the flow stress by a corresponding amount.

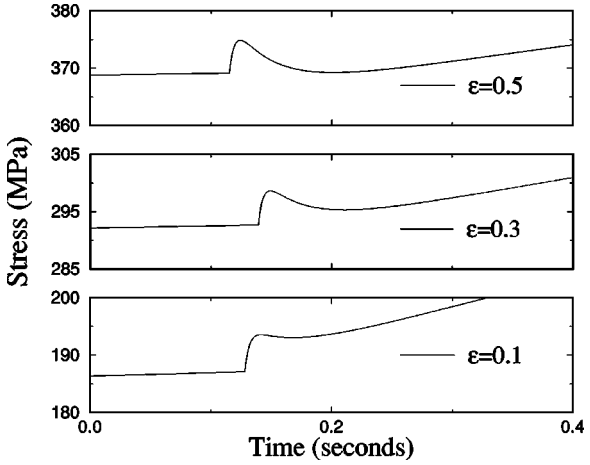

FIG. 13. Simulation showing the stress transients that accompany a sudden change in pulling speed at three different strains. The strain-rate sensitivity is initially positive, becoming negative at large strains.

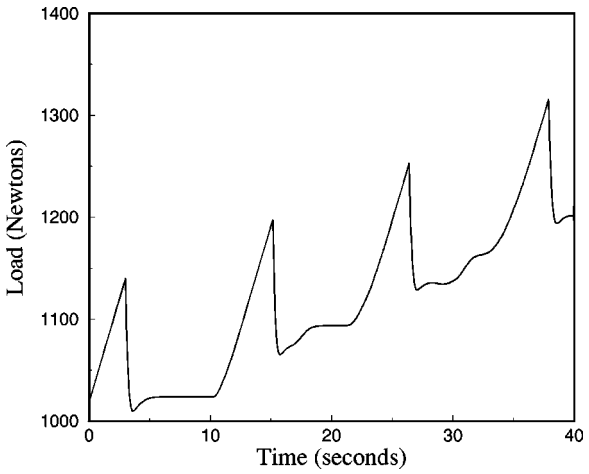

FIG. 14. Simulation results showing the stress drops due to successive fronts. Each appears at a higher yield stress, dropping to a constant as the front travels.

E. Successive fronts

1. Continuously moving fronts

The Portevin–Le Chatelier effect typically refers to the initiation and propagation of repeated yield fronts. While our model, and the analysis above, aimed at explaining the first deformation front, it nonetheless captures the phenomenon of successive fronts that propagate at ever higher stresses. Because the strain is separated into two components—''background'' strain at initiation ϵ_y and strain due solely to the current front ϵ_p—the phenomenology of successive fronts is simple.

The first front is initiated when the stress reaches the first yield value of

$$\sigma_1=\sigma_y\sqrt{\epsilon_y}. \tag{43}$$

Once the front has passed through the sample, the strain everywhere has been increased by an amount $\delta\epsilon$ and, because the sample has hardened, flow has everywhere stopped. The flow stress is then everywhere

$$\sigma_f=\sigma_y\sqrt{\epsilon_y+\delta\epsilon}. \tag{44}$$

As all plastic flow has stopped, further extension of the sample results in an increase in the stress as per Hooke's law. A second front is initiated once the stress reaches the new flow stress. By redefining the background strain to include the strain from the first front ($\epsilon_y\equiv\epsilon_y+\delta\epsilon$) the equations governing the second front become identical to those of the first front. The only difference is the larger value of the background strain ϵ_y which results in a larger strain jump $\delta\epsilon$. This behavior is shown in Fig. 14 where a constant pulling speed produces a succession of yield fronts, each with its own stress decay and propagation (at different stresses).

Since the only difference between successive fronts is the value of ϵ_y, it is fortunate that the strain jump $\delta\epsilon$ takes such a simple form, to first order

$$\delta\epsilon=2\tilde{\epsilon}_c\epsilon_y. \tag{45}$$

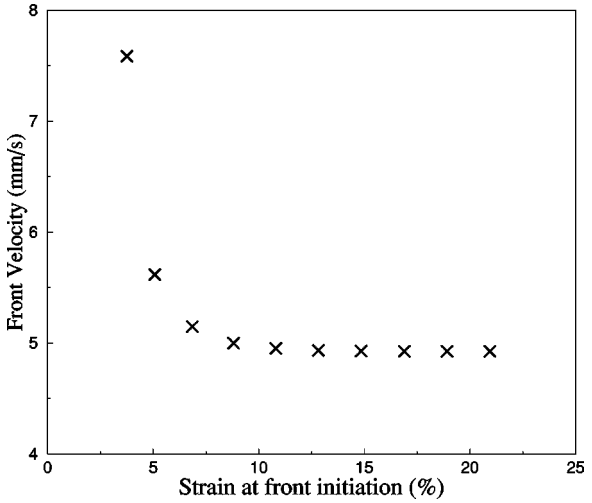

FIG. 15. Velocity versus initiation or ''background'' strain for a constant pulling speed. Successive fronts travel more slowly than earlier fronts.

The strain jump across the first front is $2\tilde{\epsilon}_c\epsilon_y$, across the second front $2\tilde{\epsilon}_c\epsilon_y(1+2\tilde{\epsilon}_c)$, and across the nth front

$$\delta\epsilon_n=\epsilon_y\sum_{i=1}^{i=n}(2\tilde{\epsilon}_c)^i. \tag{46}$$

$\tilde{\epsilon}_c$ is less than one and so this series rapidly converges to a constant

$$\delta\epsilon_\infty=\epsilon_y\frac{2\tilde{\epsilon}_c}{1-2\tilde{\epsilon}_c}\approx\frac{\epsilon_y}{2}. \tag{47}$$

The velocity at a constant pulling speed $\dot{X}$ (derived above) is

$$v=\frac{\dot{X}}{\delta\epsilon}. \tag{48}$$

The front velocity of successive fronts therefore also converges to a constant value of approximately $2\dot{X}/\epsilon_y$. This is shown in Fig. 15.

2. Hopping fronts

The above analysis is for continuously propagating bands where the velocity is set by the relation

$$v=\frac{\dot{X}}{\delta\epsilon}. \tag{49}$$

When the fronts hop, their velocity is determined directly by the pulling speed, the primary factor being how long it takes the sample to reload. If the difference between the upper and lower stress is $\Delta\sigma$ and the pulling speed $\dot{X}$ then the time to reload t is

$$t=\frac{\Delta\sigma}{\mu\dot{X}}. \tag{50}$$

Since the sample yields at a stress of $\sigma_y\sqrt{\epsilon_y}$ and falls to a value of $\sigma_y\sqrt{\epsilon_y}(1-\tilde{\epsilon}_c)$, the difference $\Delta\sigma$ is

$$\Delta\sigma=\sigma_y\sqrt{\epsilon_y}-\sigma_y\sqrt{\epsilon_y}(1-\tilde{\epsilon}_c)=\sigma_y\sqrt{\epsilon_y}\tilde{\epsilon}_c. \tag{51}$$

Successive fronts have larger background strains and therefore larger $\Delta\sigma$. As this difference increases, the reloading time also increases, and the front velocity decreases. As $\delta\epsilon_y$ approaches a constant, the velocity of hopping fronts also decreases to constant. McCormick [23] has measured the velocity of successive hopping fronts and finds the velocity decreases at higher strains, seemingly approaching a constant value.

V. CONCLUSION

We have presented a one-dimensional model that appears to capture most of the salient features of inhomogeneous plastic yielding. The foundation of this model is a modification of the flow stress to depend upon a new quantity, the ''nonlocal strain rate.'' Theory and experiment are seen to agree on many points, including the following.

(1) Fronts move steadily under a constant applied stress.

(2) Front velocity is proportional to applied pulling speed (strain jump independent of pulling speed).

(3) At low pulling speeds fronts cease to move steadily and ''hop.''

(4) Successive fronts move more slowly than their predecessors and introduce a larger strain.

(5) Stress at which fronts move rises rapidly with pulling speed before leveling off to an almost constant value.

(6) Stress drops accompanying yielding are exponential.

(7) Homogeneously deforming samples show negative strain-rate sensitivity at large strains.

Many theories claim to explain deformation fronts, and determining which is correct requires appeal to experiment. We feel there are strong reasons for believing our phenomenology is more correct than others. Ours is the only theory that produces fronts moving at a constant stress, a behavior observed in our experiments. This is an important point, one which must be emphasized strongly. The close quantitative agreement between theoretical predictions and experimental observations (e.g., Figs. 8, 9, and 10) is also unique to our phenomenology. Finally, we can extend our theory to explain experimental observations made on homogeneously deforming materials.

ACKNOWLEDGMENTS

H. Swinney and W. McCormick have provided many invaluable suggestions. We also thank Y. Estrin and O. Richmond for encouraging us to work on this problem, S. Kyriakides and K. Liechti, for allowing us use of their hydraulic testing machines, and A. Arzoumanidis for his help in working with it. We are grateful to D. Lege of Alcoa for providing us with aluminum samples. This research was supported in part by the Alcoa Foundation and the National Science Foundation (Grant No. DMR-9531187). The work of F. M. was supported by a grant from the Alexander von Humboldt Foundation.

[1] F. Mertens, S. V. Franklin, and M. Marder, Phys. Rev. Lett. **78**, 4502 (1997).
[2] A. Portevin and F. Le Chatelier, C. R. Hebd. Seances Acad. Sci. **176**, 507 (1923).
[3] F. A. von Gerstner, Ann. Chim. Phys. **26**, 269 (1832).
[4] F. Savart, Ann. Chim. Phys. **65**, 337 (1837).
[5] A. M. Masson, Ann. Chim. Phys. **3**, 451 (1841).
[6] A. H. Cottrell, Philos. Mag. **44**, 829 (1953).
[7] J. Bell, *Mechanics of Solids* (Springer-Verlag, Heidelberg, 1973), Vol. 1.
[8] Y. Estrin and L. P. Kubin, Mater. Sci. Eng., A **137**, 125 (1991).
[9] S. V. Franklin, Doctoral thesis, The University of Texas at Austin, 1997.
[10] S. H. van den Brink, A. van den Beukel, and P. G. McCormick, Phys. Status Solidi A **30**, 469 (1975).
[11] P. G. McCormick, Acta Metall. **36**, 3061 (1988).
[12] P. G. McCormick and C. P. Ling, Acta Metall. Mater. **43**, 1969 (1995).
[13] P. Penning, Acta Metall. **20**, 1169 (1972).
[14] A. Rosen and S. R. Bodner, J. Mech. Phys. Solids **15**, 47 (1966).
[15] S. R. Bodner and A. Rosen, J. Mech. Phys. Solids **15**, 63 (1966).
[16] C. P. Ling and P. G. McCormick, Acta Metall. Mater. **38**, 2631 (1990).
[17] S. V. Franklin and M. Marder, in *Plastic and Fracture Instabilities in Materials*, edited by N. Ghoniem (ASME, New York, 1995), p. 133.
[18] H. M. Zbib and E. C. Aifantis, Scr. Metall. **22**, 1331 (1988).
[19] Y. Estrin, Scr. Metall. Mater. **29**, 9 (1993).
[20] W. N. Sharpe, Jr., J. Mech. Phys. Solids **14**, 187 (1966).
[21] The fact that the jump distance appears to be determined by the sample thickness suggests motion in three dimensions. We neither expect nor find close quantitative agreement between our 1D theory and experiment in this area. Nevertheless, the instability present in the 1D equations may still be the mechanism behind the hopping fronts. 3D simulations that account for necking are needed to answer this question.
[22] K. Chihab, Y. Estrin, L. P. Kubin, and J. Vergnol, Scr. Metall. **21**, 203 (1987).
[23] P. G. McCormick, S. Venkadesan, and C. P. Ling, Scr. Metall. Mater. **29**, 1159 (1993).